# Toward a taxon-specific parameterization of bio-optical models of primary production: A case study in the North Atlantic

Hervé Claustre, Marcel Babin, Davy Merien, Joséphine Ras, Louis Prieur, and Serge Dallot

Observatoire Océanologique de Villefranche, Laboratoire d'Océanographie de Villefranche, UMR 7093, Villefranche-sur-mer, France

Ondrej Prasil and Helena Dousova

Photosynthesis Research Center, Institute of Microbiology AVCR and University of South Bohemia, Trebon, Czech Republic

Thierry Moutin

Laboratoire d'Océanographie et de Biogéochimie, UMR 6535, Centre d'Océanologie de Marseille, Marseille, France

Received 30 July 2004; revised 4 February 2005; accepted 14 April 2005; published 7 July 2005.

[1] As part of the Programme Océan Multidisciplinaire Méso Echelle (POMME) in the North Atlantic, an extensive data set of high-pressure liquid chromatography pigment concentrations, phytoplankton absorption coefficients, primary production measurements, and $P$ versus $E$ curves has been acquired. This data set is analyzed with the objective of testing whether photosynthetic performances of natural phytoplankton communities are related to taxonomic characteristics. This objective is addressed in two ways. The first approach concerns the bulk photosynthetic performances of the water column: the water column photosynthetic cross section, $\psi^*$, equals 0.088 $m^2$ gChl$a^{-1}$, i.e., ~25% higher than the average for the world ocean. Using multiple regression, size-specific values of $\psi^*$ are subsequently derived: carbon storage by water column is more efficient with microphytoplankton ($\psi^*$ = 0.135 $m^2$ gChl$a^{-1}$) than with nanophytoplankton (0.089 $m^2$ gChl$a^{-1}$) or picophytoplankton (0.064 $m^2$ gChl$a^{-1}$). The second (independent) approach examines the correlations between photophysiological properties and several abiotic and biotic variables. The correlations are weak, if any, between photophysiological properties and abiotic factors (temperature, nitrate concentration, and irradiance), while significant correlations are reported with biotic factors (proportion of the different phytoplankton groups, average size of the phytoplankton assemblage). Our results suggest that when large phytoplankton populations predominate at the expense of smaller ones, the specific absorption coefficient is expectedly lower, while other photophysiological properties $\alpha^B$, $P^B_{max}$, and $\Phi_{cmax}$, are higher. The agreement between both independent approaches points out that large phytoplankton (essentially diatoms) are potentially more efficient in carbon storage than any other phytoplankton groups on a chlorophyll $a$ or light absorption basis.

**Citation:** Claustre, H., M. Babin, D. Merien, J. Ras, L. Prieur, S. Dallot, O. Prasil, H. Dousova, and T. Moutin (2005), Toward a taxon-specific parameterization of bio-optical models of primary production: A case study in the North Atlantic, *J. Geophys. Res.*, *110*, C07S12, doi:10.1029/2004JC002634.

## 1. Introduction

[2] Bio-optical models developed for the estimation of marine primary production $P$ (g C $m^{-3}$ $s^{-1}$), and often used with remotely sensed ocean color data, are of the general form

$$P = 12\ \mathrm{PAR}[\mathrm{Chl}a]a^*\Phi_c, \quad (1)$$

with PAR (mole quanta $m^{-2}$ $s^{-1}$) being the photosynthetic available radiation, [Chl$a$] (mg $m^{-3}$) the chlorophyll $a$ concentration, $a^*$ ($m^2$ mg Chl$a^{-1}$), the [Chl$a$]-specific absorption coefficient, and $\Phi_c$ (mole carbon mole quanta$^{-1}$) the quantum efficiency for carbon fixation. The factor 12 allows for the conversion of moles into grams of carbon. It is generally recognized that the variance in $P$ is essentially driven by the product PAR [Chl$a$] [*Platt and Sathyendranath*, 1988].

[3] The estimation of PAR or [Chl$a$] is not an issue. These variables can be estimated with reasonable accuracy, even at the global scale, by measurement or modeling. The


0148-0227/05/2004JC002634$09.00

estimation of the second-order source of variance in $P$, the product $a^* \Phi_c$, is more challenging. As a first approximation, statistical relationships that relate $a^*$ [*Bricaud et al.*, 1995] and $\Phi_c$ [*Wozniak et al.*, 1992] to [Chl*a*] can be used. While such relationships reproduce average trends, they remain nevertheless limited in accounting for the natural variability of $a^*$ and $\Phi_c$.

[4] The dependence of phytoplankton bio-optical and photophysiological properties on abiotic factors, such as light, temperature and nutrients has been extensively documented from laboratory experiments [e.g., *Sakshaug et al.*, 1989; *Geider et al.*, 1996; *Stramski et al.*, 2002] and only partially in the field [e.g., *Cleveland et al.*, 1989; *Babin et al.*, 1996; *Bouman et al.*, 2003; *Maranon et al.*, 2003]. The laboratory studies have served as a basis for the development of parameterizations, sometimes empirical, that have been implemented in primary production models. This is, for example, the case for temperature [e.g., *Morel*, 1991] or, more recently for light and nutrients [*Behrenfeld et al.*, 2002]. These parameterizations, however, are not fully satisfactory. They have generally been established on well controlled (monospecific) cultures by studying the effect of one forcing variable (the others being kept constant) on the photophysiological or bio-optical responses. These parameterizations can hardly represent natural conditions where concurrent variations of environmental forcing is the rule. The physiological responses to these forcing are nonlinear, involve feedback processes and are thus highly complex. Therefore the accurate and realistic representation of physiological variability in bio-optical models essentially remains a nonresolved issue [*Behrenfeld et al.*, 2002; *Sorensen and Siegel*, 2001].

[5] At any time and location, the composition of the phytoplankton community can be considered as the integrator not only of the influence of various abiotic factors but also of the spatiotemporal occurrence of these forcings (including, for example, intermittency in light and nutrient supply which have an impact on the environmental history of phytoplankton). For example, prochlorophytes predominate in the highly stratified and nutrient depleted environments of the subtropical gyres [e.g., *Partensky et al.*, 1999] while diatoms are generally the dominant group in highly dynamic and nutrient replete upwelling systems.

[6] If the concurrent influence of abiotic factors on photosynthetic performances are difficult to explicitly implement in biophysical or physiological models, one alternative would therefore be to index these performances on the composition of phytoplankton communities. Some studies [*Claustre et al.*, 1997; *Hashimoto and Shiomoto*, 2002] have indeed suggested that the efficiency of a water column for photosynthetic carbon fixation could be dependant on the composition of the phytoplankton assemblage. To date however, no in situ investigation has clearly attempted to quantitatively infer photo physiological parameters from the knowledge of phytoplankton community composition. It is thus the main purpose of the present investigation to test whether photophysiological and bio-optical properties and water column efficiency for carbon fixation are related to the composition of phytoplankton communities.

[7] For bio-optical properties, we already have some indications about the relationship with the composition of phytoplankton communities. For example, $a^*$ can be inferred from the community composition. Numerous studies have indeed shown that variability of $a^*$ is essentially driven by the so-called package effect which is mainly affected by the size of the phytoplankton assemblage [*Bricaud et al.*, 2004]. It is recognized that oceanic areas with high chlorophyll *a* concentrations are indeed associated with large phytoplankton, and vice versa [*Chisholm*, 1992; *Claustre*, 1994]. Thus the *Bricaud et al.* [1995] parameterization between $a^*$ and [Chl*a*] implicitly relies on a relationship between community composition (or size distribution of the phytoplankton assemblage) and [Chl*a*]. By contrast, and to our best knowledge, no clear relationships have been established to date between $\Phi_c$ and, more generally, the parameters of the $P$ versus $E$ curves and phytoplankton community composition. The parameterization of *Wozniak et al.* [1992] implies that $\Phi_c$, through its maximal value $\Phi_{c\max}$, is high at elevated [Chl*a*] and low in oligotrophic regimes. This observation would suggest that large phytoplankton (e.g., diatoms) have higher $\Phi_c$ than small phytoplankton (e.g., picoplankton).

[8] The lack of comprehensive in situ investigations in the past linking taxonomic to photosynthetic performances essentially resides in the difficulty of acquiring quantitative and reliable data on phytoplankton community composition, especially over the whole size range of natural populations ($\sim$0.5–200 $\mu$m). This would require enumeration of phytoplankton populations (cytometry for small groups, microscopy for larger ones) combined with an estimation of their size and a use of appropriate conversion factors to derive biomass. This is a tedious task, highly sensitive to the choice of conversion factors and, in any case not easy to implement on a routine basis.

[9] A single high-performance liquid chromatography (HPLC) analysis provides the concentration of a suite of pigments ranging from the specific pigments of the tiny *Prochlorococcus* to the largest diatoms. Various methods have subsequently been proposed to quantify the biomass of the main phytoplankton population [*Gieskes et al.*, 1988; *Bustillos-Guzman et al.*, 1995; *Mackey et al.*, 1996] or to derive chlorophyll a associated with specific size ranges [*Claustre*, 1994; *Vidussi et al.*, 2001; *Bricaud et al.*, 2004; J. Uitz et al., From surface chlorophyll *a* to phytoplankton community composition in oceanic waters, submitted to *Limnology and Oceanography*, 2005, hereinafter referred to as Uitz et al., submitted manuscript, 2005]. Such pigment-based methods offer the quantitative basis to evidence a potential relationship between photophysiological properties and phytoplankton community composition. This is the approach we applied in the present study.

[10] We used an extensive database (HPLC pigment data, $P$ versus $E$ curves, phytoplankton absorption measurements, in situ primary production measurements) acquired as part of an intensive investigation undertaken in 2001 in the northeast Atlantic in the frame of the Programme Océan Multidisciplinaire Méso Echelle (POMME) [*Mémery et al.*, 2005]. The sampling was performed during three main periods encompassing the range of seasonal hydrodynamical and biogeochemical conditions prevailing in this area: (1) winter mixing with biological production limited by light, while the system is nutrient replete; (2) onset of stratification and beginning of the spring bloom; (3) sum-

mer stratification and associated oligotrophy. As a result of the spatial and temporal diversity of conditions covered by the present study, it was expected that the analysis of the data set would allow to draw more general inferences, more specifically the following: (1) what are the advantages of taxonomic-based parameterizations of bio-optical models when compared to "classical" models with parameterizations relying on the dependence of photophysiology on abiotic factors? (2) Is it possible to embed a taxonomic-dependant parameterization in bio-optical models?

## 2. Material and Methods

### 2.1. Investigation Zone and Sampling Strategy

[11] The investigated area, a rectangle of 500 km longitude by 750 km latitude is centered at 41.5°N, 19°W between the Iberian Peninsula and the Azores Archipelago. It encompasses the so-called discontinuity zone, which corresponds to a transition zone between two main areas; the northern part is characterized by a deep late winter mixed layer (up to 500 m), while shallow (100–150 m) winter mixed layers are observed in the southern part [*Paillet and Arhan*, 1996]. At the basin scale, these hydrological differences have marked implications on the timing as well as on the intensity of the spring bloom [*Siegel et al.*, 2002]. In addition, this part of the northeast Atlantic is subjected to a significant mesoscale activity (current meandering, presence of eddies), which is expected to impact both the magnitude and the quality (taxonomic composition) of primary production.

[12] Within the POMME domain, and with the objective of covering the three main hydrological and biogeochemical conditions, the sampling strategy was based on three ~55 day cruises during 2001. Each cruise was subdivided into two legs. The first legs were devoted to a quasi-synoptical survey of the area. They consisted in a network of ~80 conductivity-temperature-depth (CTD) rosette stations (spaced by 30 nautical miles) for the measurement of core hydrological and biogeochemical properties. The second legs were focused on process studies at four stations. These stations were chosen, on the basis of the LEG 1 synoptical survey associated with quasi real-time data assimilation and modeling, to resolve the range of variability in mesoscale structures (fronts, meanders, gyres) typical of this area. These stations were intensively sampled for biogeochemical stocks and rate measurements over 2 day periods each.

### 2.2. Light and Hydrological Measurements

[13] For POMME 1 (3 February–19 March) and POMME 2 (24 March–3 May) onboard the R/V *L'Atalante*, meteorological data were acquired using an instrumented mast equipped with an Eppley pyranometer to measure total sun radiation [*Caniaux et al.*, 2005], from which Photosynthically Available Radiation was derived. For POMME3 (26 August–8 October) onboard the R/V *Thalassa*, total sun radiation derived from METEOSAT data was obtained from the Spatial Meteorological Center (Lannion, France). Fluxes were hourly resolved with a spatial resolution of 0.04 degrees of longitude/latitude [*Caniaux et al.*, 2005]. In addition, PAR at the sea surface under clear sky was derived as by *Morel* [1991].

[14] The depth of the mixed layer, $Z_m$ (m), was estimated from excess density profiles derived from CTD casts. It corresponds to the depth where the density is higher than the surface one by more than 0.02 kg $m^{-3}$. The depth of the euphotic layer, $Z_e$ (m), defined as the depth where irradiance is reduced to 1% of its surface value, was estimated according to *Morel and Berthon* [1989] using the [Chl*a*] vertical profiles. The statistical relationships presented by *Morel and Berthon* [1989] and linking *Ze* to the integrated content in Chlorophyll *a*, $\langle \text{Chl}a \rangle$, were updated using the parameterization proposed by *Morel and Maritorena* [2001]. The ratio of the geometrical depth, *Z*, to *Ze* (*Z*/*Ze*, dimensionless) is also used as an optical depth.

### 2.3. Absorption and Pigment Measurements and Data Reduction

[15] For the measurements of pigment concentrations and particulate absorption coefficients, 2.8 L of seawater were filtered onto 25 mm Whatman GF/F glass-fiber filters. The optical density of the filter was subsequently monitored over the 370–750 nm spectral range using a LICOR spectroradiometer (LI-1800) equipped with an integrating sphere. The spectral absorption coefficient of phytoplankton, $a_\phi(\lambda)$ ($m^{-1}$) was derived as described by *Claustre et al.* [2000].

[16] Immediately after the optical density measurement, the filters were stored in liquid nitrogen until laboratory analysis of pigments. Samples were extracted in 3 mL HPLC-grade methanol and injected into a reversed phase C8 Hypersil MOS column (dimensions of 3 × 100 mm, 3 μm pore size) and analyzed with an Agilent Technologies 1100 series HPLC system coupled to a Thermoquest AS3000 autosampler. The HPLC procedure derived from the protocol of *Vidussi et al.* [1996] is detailed by *Claustre et al.* [2004]. Precision of the method averaged 5% and the detection limit for chlorophyll *a* and a carotenoid, fucoxanthin, was 0.001 mg $m^{-3}$.

[17] Several methods have been proposed to retrieve quantitative information on size structure of the communities using HPLC pigment concentrations. *Claustre* [1994] proposed a criterion that represents the proportion of microphytoplankton (20–200 μm) within a phytoplankton community. This approach was thereafter extended by *Vidussi et al.* [2001] to derive the [Chl*a*] associated with three main phytoplankton size classes (pico- (<2 μm), nano- (20–200 μm) and microphytoplankton). This study assumed that the taxonomic pigment/Chl*a* ratio was identical for all phytoplankton populations, an assumption that was not strictly realistic [*Vidussi et al.*, 2001]. *Vidussi et al.*'s [2001] approach was recently revisited and improved on the basis of the analysis of a large pigment database by Uitz et al. (submitted manuscript, 2005). The variability in the taxonomic pigment/Chl*a* ratio according to the various populations is now taken into account and thus the biomass proportion of the three main phytoplankton size classes more accurately determined. The equation allowing the retrieval of these size fractions have recently been published by *Bricaud et al.* [2004]. Additionally *Bricaud et al.* [2004] derived a phytoplankton size index, SI (μm), by giving a central size value to each class (1 μm, 5 μm and 50 μm for pico-, nano-, and microphytoplankton, respec-

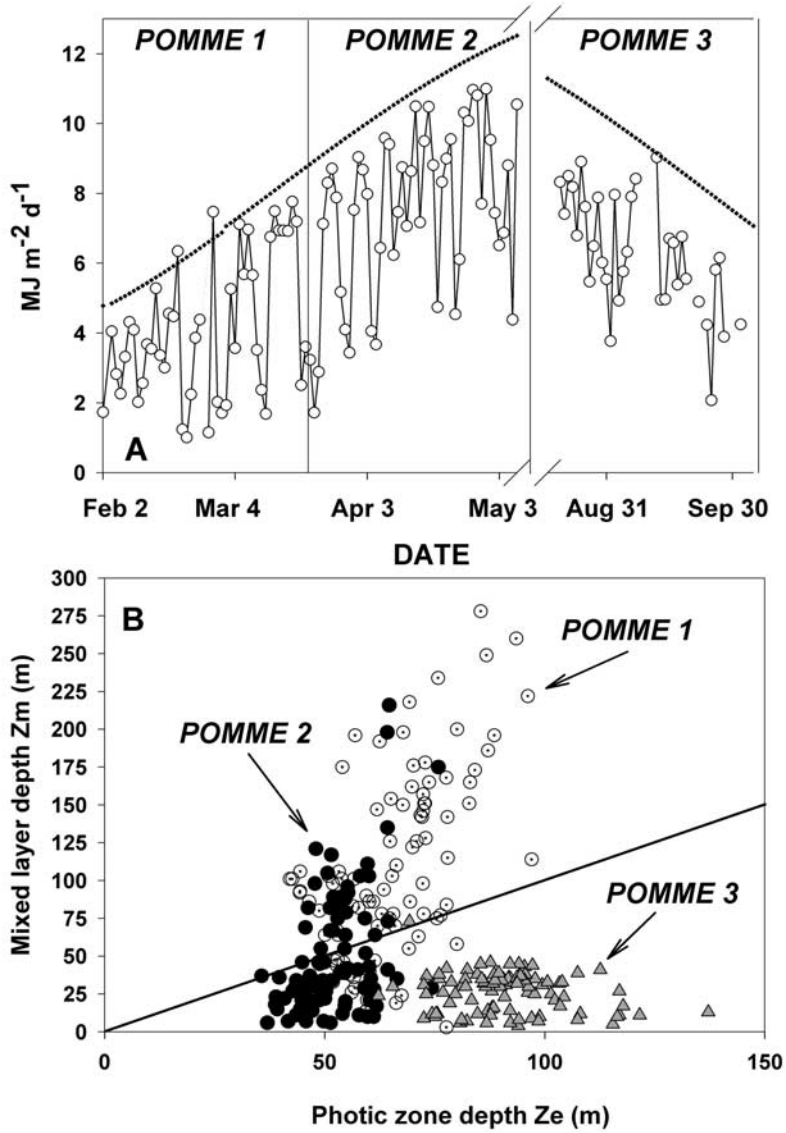


**Figure 1.** Light and hydrological context during the three Programme Océan Multidisciplinaire Méso Echelle (POMME) cruises in the eastern North Atlantic in 2001. (a) Clear-sky modeled (dotted line) and measured (open circle) surface daily irradiance. Only consecutive daily measurements are connected (solid line). (b) Relationship between the depth of the euphotic layer, *Ze*, and the depth of the mixed layer, *Zm*. The line identifies the domain where $Ze = Zm$.

tively) and weighting by the biomass proportion of each class.

### 2.4. Photosynthesis-Irradiance Curves (*P* Versus *E*)

[18] The parameters of the relationship between carbon fixation by phytoplankton and irradiance (so-called *P* versus *E* curve) were determined as described by *Babin et al.* [1996]. Briefly, after inoculation with inorganic $^{14}C$ ($NaH^{14}CO_3$, ~0.4 μCi/mL, Amersham®), each sample was subdivided into 12 50 mL subsamples and incubated for ~2 hours at different light levels in a radial photosynthetron described by *Babin* [1994]. To determine the initial activity, three aliquots of 25 μL were taken immediately after inoculation and added to 50 μL of an organic base (ethanolamin), 1 mL of distilled water and 10 mL of the scintillation cocktail (Packard®, Aquasol-2). The photosynthetically available radiation (PAR) at each position in the incubation chambers was measured using a quantum scalar irradiance meter (Biospherical® Instruments, QSL100). Temperature in the incubation chambers was maintained at in situ temperature (±1°C) using thermoregulated water circulating baths. After incubation, subsamples were filtered under low vacuum onto glass fiber filters (Whatman®, GF/F, 25 mm), wetted with 1 mL of HCl 1N, kept under a fuming hood for 1 hour, and placed into 10 mL of scintillation cocktail. Activity was measured in the laboratory using a liquid scintillation counter (Packard®, Minaxi Tricarb Serie 4000), and the carbon fixation rate was calculated as by *Parsons et al.* [1984] and normalized to [Chl*a*] to obtain $P^B$ [mg C (mg Chl*a*)$^{-1}$ h$^{-1}$].

[19] The initial slope of the *P* versus *E* curve [$\alpha^B$, mg C (mg Chl*a*)$^{-1}$ h$^{-1}$ (μmol quanta m$^{-2}$ s$^{-1}$)$^{-1}$] and the

**Table 1.** Summary of Seasonal Variations in Phytoplankton Biomass and Community Composition Over the Euphotic Layer[a]

| | Winter (95) | Spring (91) | Summer (94) |
|---|---|---|---|
| $\langle \text{Chl}a \rangle$, mg m$^{-2}$ | 24.3 ± 5.6 | 31.4 ± 5.6 | 16.0 ± 2.7 |
| Pico, % | 43.8 ± 10.3 | 22.4 ± 10.9 | 52.6 ± 9.6 |
| Nano, % | 46.0 ± 7.2 | 59.3 ± 13.9 | 39.6 ± 7 |
| Micro, % | 10.2 ± 3.6 | 18.3 ± 9.8 | 7.8 ± 6.5 |

[a]The number in parentheses refers to the number of pigment profiles sampled.

maximum chlorophyll-specific carbon fixation rate [$P^B_{\max}$, mg C (mg Chl$a$)$^{-1}$ h$^{-1}$] were estimated by fitting the expression proposed by *Platt et al.* [1980] to the experimental $P^B$ and PAR data. The saturation parameter $E_K$ (μmol quanta m$^{-2}$ s$^{-1}$) was calculated as

$$E_K = \frac{P^B_{\max}}{\alpha^B}. \quad (2)$$

The maximum quantum yield of carbon fixation [$\Phi_{c\max}$, mol C (mol quanta)$^{-1}$] was derived from

$$\Phi_{c\max} = \frac{\alpha^B}{\overline{a}^*}, \quad (3)$$

where $\overline{a}^*$ is the average chlorophyll-specific absorption coefficient of phytoplankton weighted by the spectral irradiance inside the incubations chambers [$E(\lambda)$]:

$$\overline{a}^* = \frac{\int_{400}^{700} a^*(\lambda)E(\lambda)d\lambda}{\int_{400}^{700} E(\lambda)d\lambda}. \quad (4)$$

$E(\lambda)$ was taken from *Babin* [1994].

### 2.5. Primary Production Measurements

[20] In situ primary production measurements were performed exclusively during the Leg 2 of the 3 cruises (four vertical profiles per cruise). The rate of carbon fixation was quantified using the $^{14}$C method according to the experimental protocol detailed by *Moutin and Raimbault* [2002]. Samples (320 mL polycarbonate bottles, three light and one dark sample per depth, seven to eight depths) were collected before sunrise using 12 L Niskin bottles, inoculated with 20 μCi of NaH$^{14}$CO$_3$ (Amersham CFA3) just before sunrise, and then incubated in situ. After 24 hours, the samples were filtered onto 25 mm GF/F filters to measure net fixation ($A_N$, mgC m$^{-3}$). Filters were then covered with 500 μl of 0.5 M HCl and stored for counting at the laboratory. Each day, three samples were filtered immediately after inoculation for $t_o$ determination, and 250 μL of sample was taken at random from three bottles and stored with 250 μL of ethanolamine to determine the quantity of added tracer ($Q_i$). In the laboratory, samples were dried during 12 hours at 60°C, 10 mL of ULTIMAGOLD-MV (Packard) were added to the filters and the activity was determined after 24 hours using a Packard Tri carb 2100 TR liquid scintillation counter.

[21] Daily (24 hours, dawn to dawn) primary production ($P$, mg C m$^{-3}$ s$^{-1}$) was obtained from the difference between light and dark bottle measurements. Areal primary production ($\langle P \rangle$, g C m$^{-2}$ d$^{-1}$) was calculated assuming that (1) subsurface (about 5 m) rates are identical to surface rates (not measured) and (2) $P$ is null at 20 m below the deepest sampled depth (below the euphotic layer).

## 3. Results

### 3.1. Light and Hydrological Context at the Seasonal Scale

[22] The daily and seasonal variability in irradiance at the sea surface (Figure 1a), and in the thicknesses of mixed and euphotic layers (Figure 1b) indicate that the phytoplankton communities experienced a wide range of light forcing conditions. During summer (POMME 3), the euphotic layer (62–137 m) generally extended deeper than the mixed layer (<50 m). During POMME 1 and POMME 2, $Z_e$ and $Z_m$ were covarying ($r$ = 0.64; $n$ = 186; $p < 0.001$): the deeper the mixed layer (beginning of winter investigations), the clearer the waters (the lower the phytoplankton biomass) and reciprocally. This trend likely reflects the transition between limiting and nonlimiting light conditions in the control of phytoplankton growth and biomass accumulation (nutrients were never depleted at these periods [*Fernández et al.*, 2005]). Over the winter–spring period, the mixed layer indeed gradually decreased by a factor of ∼5 while surface irradiance was increasing by a factor ∼2 (and day length by ∼4 hours). Thus the average light received by phytoplankton cells was overall increasing, allowing the progressive biomass accumulation, hence implying a decrease in *Ze*.

### 3.2. Phytoplankton Responses at the Seasonal Scale

#### 3.2.1. Biomass and Phytoplankton Community Composition

##### 3.2.1.1. General Seasonal Evolution

[23] The end of summer (POMME 3) was clearly the period of low phytoplankton biomass while spring (POMME 2) corresponded to the period of highest biomass (Table 1, Figure 2a). Biomass levels in the winter time were intermediary. In winter, pico- and nanophytoplankton mostly equally contributed to chlorophyll *a* biomass (45% of the biomass each). During the second leg of POMME 1, there was a clear and regular increase in biomass which likely corresponds to the bloom initiation. This transition was clearly marked by an evolution in the phytoplankton community composition (Figure 2b) with microphytoplankton and nanophytoplankton biomass increasing at the expense of picophytoplankton. Later on during spring, nanophytoplankton were, on average, dominant while micro- and picophytoplankton represented the same proportion of the biomass (∼20%). At the end of the summer period, picophytoplankton was the dominant phytoplankton (∼55%) and microphytoplankton the lowest (∼7%).

##### 3.2.1.2. Vertical Pattern

[24] Clear seasonal differences were observed in the vertical distribution of the phytoplankton biomass (Figure 3). Average winter profiles display a 30–40 m homogenous biomass layer (∼0.35–0.40 mg Chl$a$ m$^{-3}$) and a regular

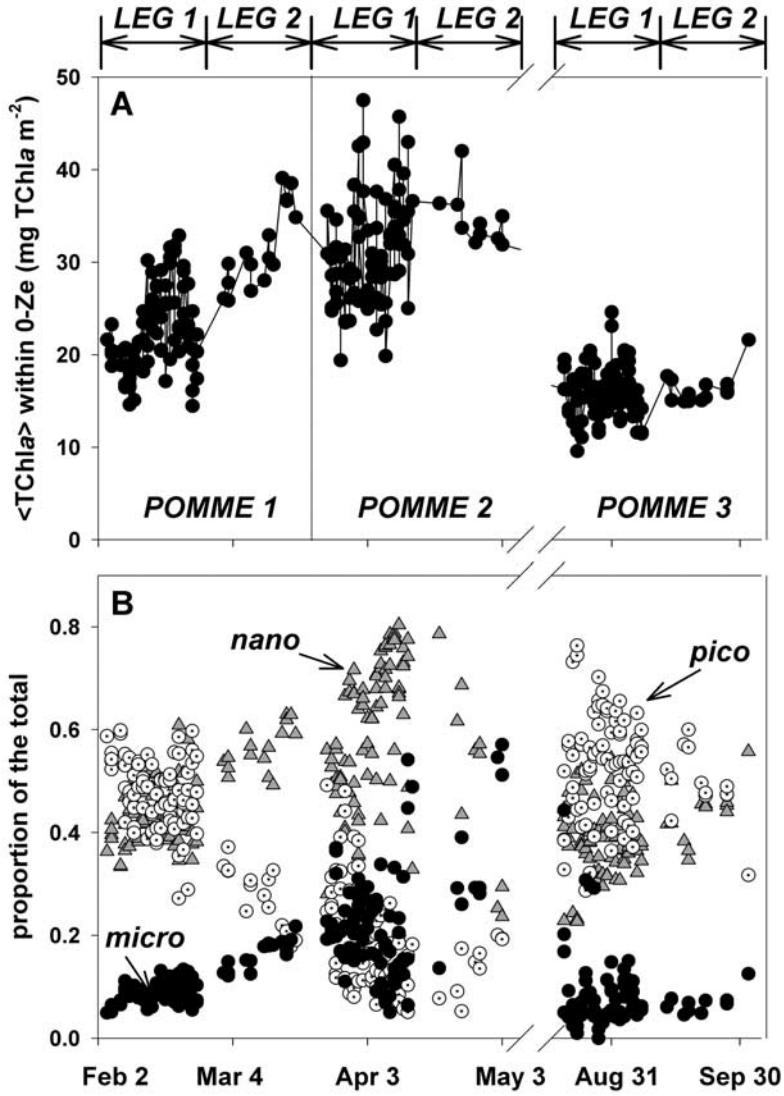


**Figure 2.** Temporal evolution of the phytoplankton biomass within the euphotic layer during the three POMME cruises in the eastern North Atlantic in 2001. (a) Integrated chlorophyll *a*, ⟨Chl*a*⟩. (b) Proportion of the three main phytoplankton size classes.

decrease down to 200 m, with the community composition remaining remarkably constant within the upper 100 m layer (Figure 3d). During spring (POMME 2), the biomass increased toward the surface (up to 0.7 mg Chl*a* $m^{-3}$, maximum recorded: 1.8 mg Chl*a* $m^{-3}$); this increase was essentially associated (on average) with nanophytoplankton which represented 60–65% of the biomass in this layer. At the end of summer, surface [Chl*a*] was low (0.08 mg Chl*a* $m^{-3}$) and was mostly due to the presence of picophytoplankton (zeaxanthin containing cyanobacteria, i.e., *Prochlorococcus* and *Synechococcus*), which represented up to 70% of the biomass in this layer (Figure 3f). At 50–60 m, a deep chlorophyll maximum (DCM) (~0.27 mg $m^{-3}$) developed with similar contributions of pico- and nanophytoplanktonic populations. Below the DCM, the increase in picophytoplankton was essentially due to the presence of DV-Chl*b* containing *Prochlorococcus*.

### 3.2.2. Primary Production

[25] Average primary production profiles (four casts performed during each LEG 2) clearly revealed (Figure 4) that the winter time is a period of significant production, surprisingly not so different from the spring one, where the bloom is expected. Actually, areal primary production in spring (825 ± 270 mg C $m^{-2}$ $d^{-1}$), was only 37% higher than for winter conditions (602 ± 193 mg C $m^{-2}$ $d^{-1}$). Summer surface primary production was extremely low (<5 mg C $m^{-3}$ $d^{-1}$), as a consequence of low biomass (Figure 3); similarly areal primary production was low with a value of 205 ± 30 mg C $m^{-2}$ $d^{-1}$, typical of highly oligotrophic conditions.

### 3.2.3. Variations of the Photophysiological Properties

[26] The spectrally averaged [Chl*a*]-specific absorption coefficient, $\overline{a}^{*}_{\Phi}$, displayed a rather homogeneous vertical distribution in winter and spring (Figure 5, Table 2). The

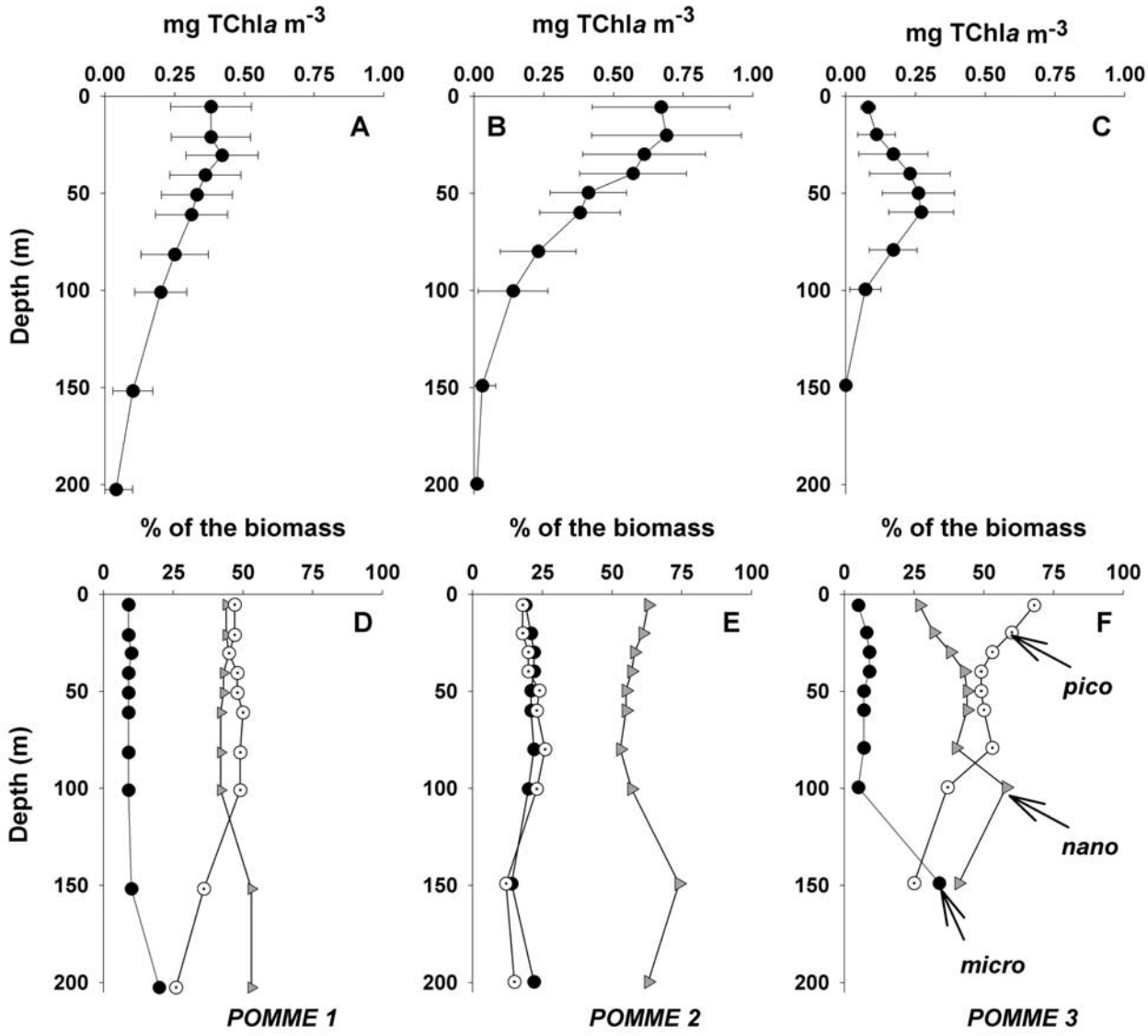


**Figure 3.** Average vertical profiles of phytoplankton biomass during the three POMME cruises in the eastern North Atlantic in 2001. (a–c) Concentration in chlorophyll *a*. (d–f) Proportion of the three main phytoplankton size classes.

lowest values were recorded in spring, when the phytoplankton assemblage was more dominated by large phytoplankton (diatoms and flagellates) than in winter. In summer, when zeaxanthin containing picophytoplankton dominated, especially in surface layers, the highest values of $\overline{a}^*_\Phi$ were recorded.

[27] The [Chl*a*] normalized maximum photosynthetic rates, $P^B_{max}$, were the highest during the spring time with maximal surface values of 3.6 mg C mg Chl$a^{-1}$ $h^{-1}$ (Figure 5b). While the winter profile of $P^B_{max}$, like the winter profile of biomass and of other photophysiological parameters, displayed a homogenous distribution with depth (between ~1.5 and ~2.0 mg C mg Chl$a^{-1}$ $h^{-1}$), the summer one presented some stratification with the highest value at the surface (2.7 mg C mg Chl$a^{-1}$ $h^{-1}$) and the lowest one at depth.

[28] The normalized, light-limited photosynthetic efficiency, $\alpha^B$, shows its highest values during spring and its lowest during summer especially in the top 20 m. This seasonal and vertical pattern was similar for the maximum quantum yield of carbon fixation, $\Phi_{Cmax}$. $\Phi_{Cmax}$ covered a wide range of variations in surface layers with the lowest values in summer (0.008 ± 0.003 mole C mole quanta$^{-1}$) and the highest ones in spring (0.048 ± 0.016 mole C mole quanta$^{-1}$) (Figure 5d). There was an overall increase (decrease) of $\Phi_{Cmax}$ with depth in summer (spring), while the winter profiles presented a homogenous vertical distribution around a central value of ~0.03 mole C mole quanta$^{-1}$. Finally, $E_k$, the irradiance value at which photosynthesis saturates, showed no significant variations with depth in winter (around a central value of 50 μm quanta $m^{-2}$ $s^{-1}$), was slightly higher at surface in

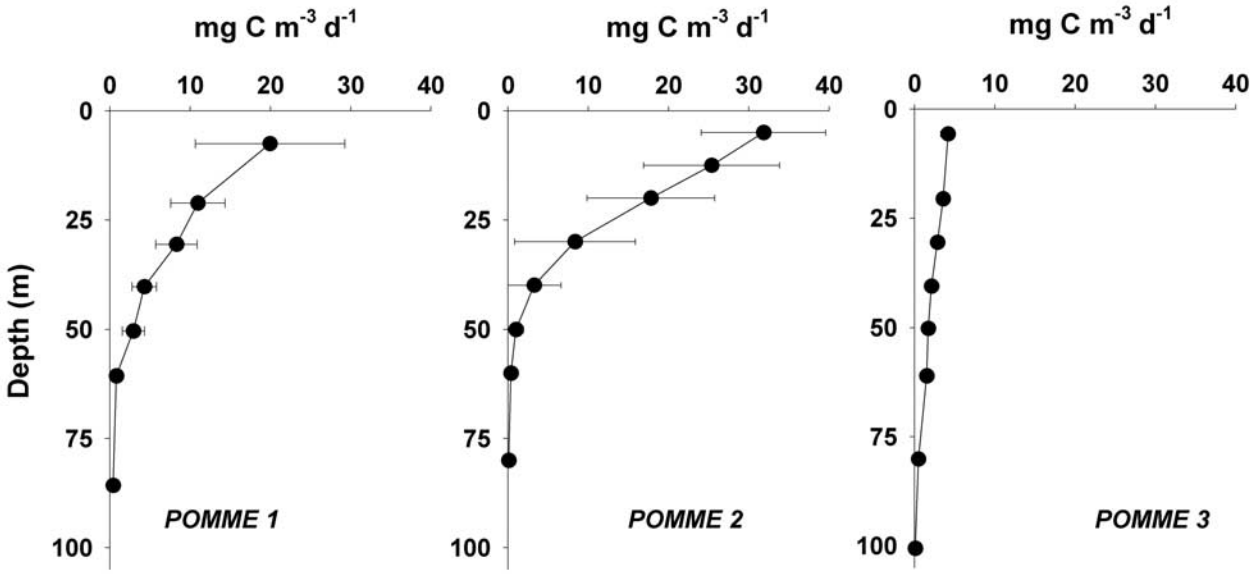


**Figure 4.** Average vertical profiles in rates of primary production during the three POMME cruises in the eastern North Atlantic in 2001.

spring, and strongly increased with depth during summer (with values up to 180 μm quanta $m^{-2}$ $s^{-1}$ in the top 20 m) (Figure 5e).

## 4. Discussion

### 4.1. Water Column Photosynthetic Cross Section and Community Composition

[29] When applied to the entire productive column (i.e., from surface to 1.5 Ze), equation (1) can be rewritten as

$$\langle P \rangle = 1/39\ \mathrm{PAR}(0^+)\psi^*\langle \mathrm{Chl}a \rangle, \qquad (5)$$

where $\langle P \rangle$ is the areal primary production expressed in g C $m^{-2}$ $d^{-1}$ $\mathrm{PAR}(0^+)$, the daily-integrated photosynthetic available radiation at the surface is now expressed in energy units (KJ $m^{-2}$ $d^{-1}$, through a conversion of 2.5 $10^{18}$ quanta $J^{-1}$ [*Morel and Smith*, 1974], the factor 39 corresponds to the energetic equivalent of 1 g of C (39 KJ g $C^{-1}$), $\langle \mathrm{Chl}a \rangle$ is the photic layer integrated chlorophyll *a* content (g Chl*a* $m^{-2}$), and Ψ* ($m^2$ g $\mathrm{Chl}a^{-1}$) corresponds to the water column cross section for carbon fixation. From the examination of equations (1) and (5), it is obvious that Ψ* can be considered as a proxy of the water column averaged product $a^*$ $\Phi_c$. Interestingly, while $a^*$ and $\Phi_c$ might present large variations [*Bricaud et al.*, 1995; *Wozniak et al.*, 1992], it has been reported that, for the global ocean, Ψ* varies within a relatively narrow range around a central value of 0.070 ± 0.035 $m^2$ g $\mathrm{Chl}a^{-1}$ [*Morel*, 1991]. This relative invariance reveals that the product $a^*$ $\Phi_c$ remains confined within a relatively narrow interval, a feature already reported by *Morel et al.* [1996].

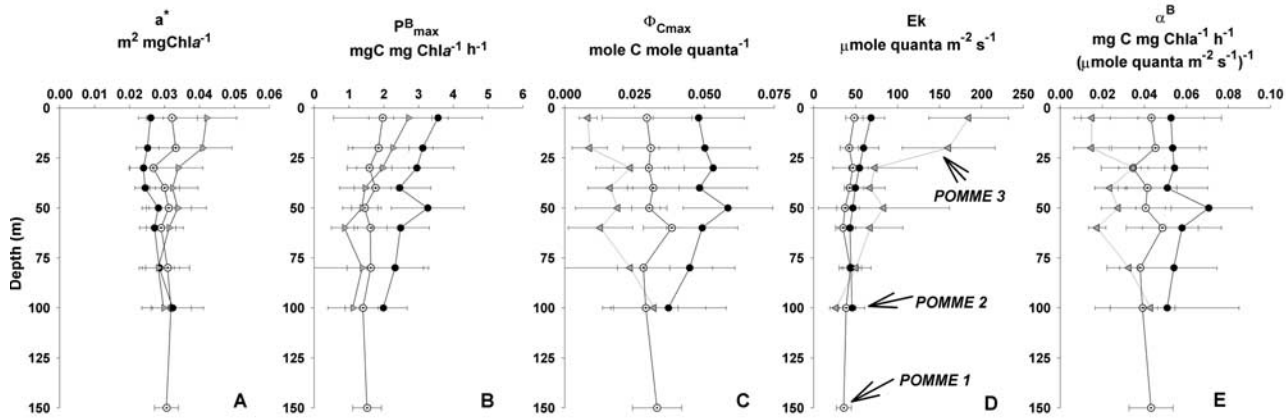


**Figure 5.** Average vertical profiles in certain bio-optical and photophysiological properties during the three POMME cruises in the eastern North Atlantic in 2001. (a) [Chl*a*]-specific absorption coefficient. (b) [Chl*a*]-normalized maximum photosynthetic rate. (c) Maximum quantum yield for carbon fixation. (d) Saturation irradiance. (e) [Chl*a*]-normalized initial slope of the $P^B$ versus $E$ curve.

**Table 2.** Summary of Seasonal Variations in Photophysiological and Community Structure Parameters or Indices Over the Euphotic Layer[a]

| | Winter (118) | Spring (139) | Summer (77) |
|---|---|---|---|
| $P^B_{max}$, mg C mg Chl$a^{-1}$ h$^{-1}$ | 1.69 ± 0.79 (118) | 2.75 ± 1.10 (139) | 1.74 ± 1.11 (77) |
| $\alpha^B$, mg C mg Chl$a^{-1}$ h$^{-1}$ (μmole quanta m$^{-2}$ s$^{-1}$)$^{-1}$ | 0.042 ± 0.021 (118) | 0.055 ± 0.02 (139) | 0.024 ± 0.021 (77) |
| $\overline{a}^*_\Phi$, m$^2$ mg Chl$a^{-1}$ | 0.031 ± 0.006 (118) | 0.027 ± 0.05 (139) | 0.035 ± 0.008 (77) |
| $\Phi_{Cmax}$, mole C mole quanta$^{-1}$ | 0.031 ± 0.011 (118) | 0.048 ± 0.017 (139) | 0.016 ± 0.014 (77) |
| Ψ*, m$^2$ g Chl$a^{-1}$ | 0.088 ± 0.020 (4) | 0.098 ± 0.001 (4) | 0.077 ± 0.017 (4) |

[a]The number in parentheses refers to the number of measurements performed.

[30] In the present study, Ψ* averaged 0.088 ± 0.017 m$^2$ g Chl$a^{-1}$ for the 12 primary production profiles determined during the three POMME cruises. Some seasonal differences in Ψ* were observed, especially when comparing the spring period, when Ψ* has the highest value, with summer period. These two periods represent the extremes in terms of phytoplankton biomass as well as community composition. The period when large phytoplankton dominates (spring) presents larger water column efficiency for carbon fixation than the oligotrophic period essentially dominated by picophytoplankton.

[31] In order to test the hypothesis of a possible size-specific dependency in ψ*, equation (5) is rewritten as

$$P = 1/39\ \mathrm{PAR}(0^+)\left[\langle_{\mathrm{pico}}\mathrm{Chl}a\rangle\Psi^*_{\mathrm{pico}} + \langle_{\mathrm{nano}}\mathrm{Chl}a\rangle\Psi^*_{\mathrm{nano}} + \langle_{\mathrm{micro}}\mathrm{Chl}a\rangle\Psi^*_{\mathrm{micro}}\right], \quad (6)$$

where $\Psi^*_{\mathrm{pico}}$, $\Psi^*_{\mathrm{nano}}$, and $\Psi^*_{\mathrm{micro}}$ represent the partial water column photosynthetic cross sections of pico-, nano-, and microphytoplankton, respectively, and $\langle_{\mathrm{pico}}\mathrm{Chl}a\rangle$, $\langle_{\mathrm{nano}}\mathrm{Chl}a\rangle$ and $\langle_{\mathrm{micro}}\mathrm{Chl}a\rangle$ correspond to size-specific [Chl$a$] integrated over the euphotic layer. $\Psi^*_{\mathrm{pico}}$, $\Psi^*_{\mathrm{nano}}$, and $\Psi^*_{\mathrm{micro}}$ were estimated through multiple regression between the dimensionless term 39 $P$/PAR($0^+$) (dependant variable) and the three size-specific $\langle$Chl$a\rangle$ (independent variables).

[32] Results from this regression reveal clear and significant trends ($r$ = 0.92, $n$ = 12, $p < 0.001$): $\Psi^*_{\mathrm{micro}}$ (0.127 ± 0.023 m$^2$ gChl$a^{-1}$) is twice higher than $\Psi^*_{\mathrm{pico}}$ (0.065 ± 0.032 m$^2$ gChl$a^{-1}$), while $\Psi^*_{\mathrm{nano}}$ presents an intermediate value (0.086 ± 0.016 m$^2$ gChl$a^{-1}$). In other words, for the same amount of chlorophyll *a* biomass within the euphotic layer, and for the same surface irradiance, carbon fixation is twice higher when diatoms dominate the community as compared to picoplankton dominated communities. This result confirms the previous study of *Claustre et al.* [1997] where, in a completely different environment (the Southern Ocean), it was shown that diatoms, with an average Ψ* of ~0.11 m$^2$ g Chl$a^{-1}$, were the most efficient primary producers compared to any other phytoplankton groups. Similar conclusions were also obtained in the subarctic Pacific by *Hashimoto and Shiomoto* [2002], who showed that light utilization efficiency, as expressed by an analog of Ψ* (Ψ, the water column light utilization index [*Falkowski*, 1981]), is higher for large phytoplankton, possibly diatoms, than for smaller phytoplankton. Typically, diatoms, and to a lesser extent nanophytoplankton, are the opportunistic species of favorable environmental (light and nutrient) conditions which prevail during spring time. In this study, picoplankton cope with low light in winter (deep mixing) and low nutrients in summer. The micro-size fraction, and to a lesser extent the nano-size fraction are the groups of the more favorable environment.

[33] This possible dependence of the water column cross section for carbon fixation on the composition of the phytoplankton community can be confirmed by a similar dependence of the photophysiological properties. This is the main purpose of the following section.

**Table 3.** Linear Correlation Coefficients Between Photophysiological and Bio-optical Parameters and Biotic or Abiotic Variables for the Three Seasons Investigated During the Programme Océan Multidisciplinaire Méso Echelle (POMME)[a]

| | Micro, % | Nano, % | Pico, % | Size | *Z*/*Ze* | *T*, deg | [$NO_3$] |
|---|---|---|---|---|---|---|---|
| | | | *Winter (POMME1)* | | | | |
| $P^B_{max}$ | −0.490 | −0.385 | 0.460 | −0.504 | | | |
| $\alpha^B$ | −0.440 | −0.329 | 0.400 | −0.450 | | | |
| $\overline{a}^*_\Phi$ | −0.558 | −0.445 | 0.529 | −0.575 | | 0.343 | |
| $\Phi_{Cmax}$ | | | | | | | |
| *Ek* | | | | | | | |
| | | | *Spring (POMME 2)* | | | | |
| $P^B_{max}$ | | | | | 0.469 | | |
| $\alpha^B$ | | | | | | | |
| $\overline{a}^*_\Phi$ | | | | | | −0.450 | 0.537 |
| $\Phi_{Cmax}$ | | | | | | | |
| *Ek* | | | | | 0.538 | | |
| | | | *Summer (POMME3)* | | | | |
| $P^B_{max}$ | | | | | 0.469 | 0.402 | |
| $\alpha^B$ | | | | | | | |
| $\overline{a}^*_\Phi$ | −0.435 | −0.417 | 0.550 | −0.480 | 0.564 | 0.562 | −0.418 |
| $\Phi_{Cmax}$ | | | | | | | |
| *Ek* | | −0.403 | 0.401 | | 0.655 | 0.524 | −0.443 |

[a]Only values which are significant at the $p$ = 0.001 level are reported.

### 4.2. Photophysiological Properties Versus Abiotic and Biotic Factors

[34] In the POMME area, the seasonal variations in the photophysiological and bio-optical properties are significant

**Table 4.** Linear Correlation Coefficients Between Photophysiological and Bio-optical Parameters and Biotic or Abiotic Variables for the Whole POMME Data Set

| | Micro, % | Nano, % | Pico, % | Size | *Z*/*Ze* | *T*, deg | [$NO_3$] |
|---|---|---|---|---|---|---|---|
| $P^B_{max}$ | 0.320 | | −0.271 | 0.325 | 0.240 | | |
| $\alpha^B$ | 0.242 | 0.312 | −0.351 | 0.269 | | −0.408 | 0.204 |
| $\overline{a}^*_\Phi$ | −0.482 | −0.429 | 0.557 | −0.515 | 0.274 | 0.445 | |
| $\Phi_{Cmax}$ | 0.443 | 0.466 | −0.566 | 0.480 | | −0.486 | |
| *Ek* | | −0.331 | 0.322 | | 0.459 | 0.655 | −0.495 |

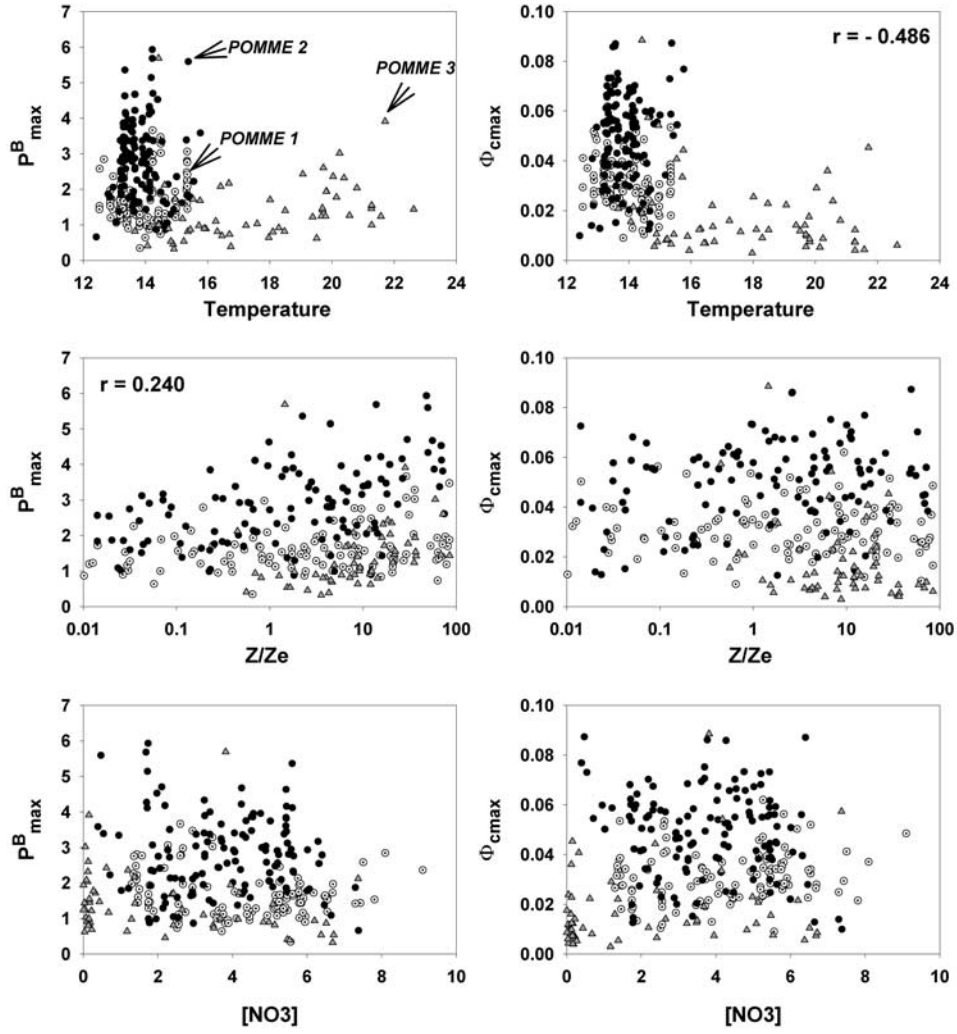


**Figure 6.** Potential relationships between two photophysiological parameters ($P^B_{max}$ and $\Phi_{cmax}$) and three abiotic factors (temperature, relative irradiance, and nitrate concentration) in the eastern North Atlantic in 2001. When significant at the $p = 0.001$ level, the linear correlation coefficients are reported in the corresponding graph.

(Figure 5). Trying to relate these variations to changes either in phytoplankton community composition or in abiotic factors (temperature, light, nutrients) essentially reveals that the correlations are primarily dependent on the scale of observation (the season or the year) (Tables 3 and 4, Figures 6 and 7).

[35] The positive correlation between $P^B_{max}$, temperature and light during summer is the result of adaptation of the phytoplankton maximal potential for photosynthesis to stable light and temperature conditions (stratified conditions) (see the regular decrease of $P^B_{max}$ over 0–75 m (Figure 5)). At the yearly scale however, $P^B_{max}$ is clearly not controlled by temperature (Table 4). This important result contradicts, at least partly, previous studies that use relationships linking $P^B_{max}$ to temperature when estimating primary production from satellite chlorophyll maps [*Behrenfeld and Falkowski*, 1997; *Antoine and Morel*, 1996]. The rationale for using such a relationship is the known temperature dependency of enzymatically driven dark reactions of photosynthesis. Some of these relationships have been derived from laboratory-controlled monospecific cultures. For natural conditions however, even if these physiological mechanisms still hold at the species level, they can be hidden by concurrent responses to other abiotic factors (light and nutrient) and by changes in species composition. At the yearly scale indeed it becomes difficult to highlight a clear response of $P^B_{max}$ to a given abiotic factor. However some trends do emerge between $P^B_{max}$ and biotic factors (Figure 7). Notably, $P^B_{max}$ (as well as $\alpha^B$) is positively related with the proportion of microphytoplankton (roughly the proportion of diatoms). At this stage, however, it is not possible to determine whether diatoms have an intrinsic $P^B_{max}$ (or $\alpha^B$) higher than other phytoplankton. This result solely reflects the observation that $P^B_{max}$ was the highest during spring time when the proportion of diatoms was the highest (Table 1, Figures 3 and 4). This property is promising in view of using community composition as an empirical predictor of $P^B_{max}$.

[36] The study of *Sorensen and Siegel* [2001], based on a 5 year observation time series in the Sargasso Sea, clearly

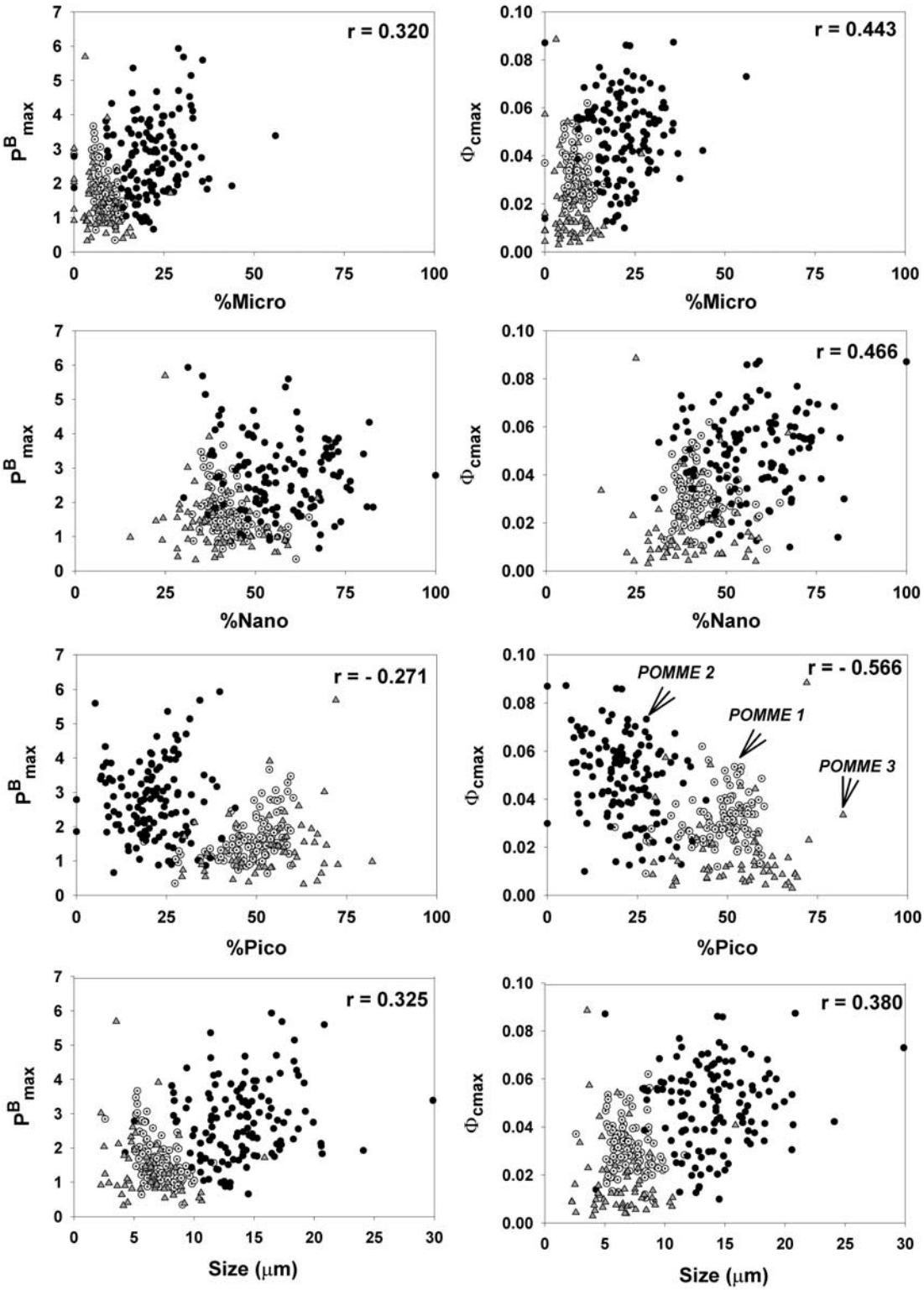


**Figure 7.** Potential relationships between two photophysiological parameters ($P^B_{max}$ and $\Phi_{cmax}$) and four biological variables (proportions and size of the phytoplankton assemblage) in the eastern North Atlantic in 2001. When significant at the $p = 0.001$ level, the linear correlation coefficients are reported.

**Table 5.** Partial Slopes of the Multiple Regression Between Non-normalized Photophysiological Parameters and Phytoplankton Biomass Variables for the Whole POMME Data Set[a]

| | Micro | Nano | Pico |
|---|---|---|---|
| $P^B_{max}$, mg C mg Chl$a^{-1}$ $h^{-1}$ | 6.27 ± 0.53 | 2.38 ± 0.23 | 0.13 ± 0.3 |
| $\alpha^B$, mg C mg Chl$a^{-1}$ $h^{-1}$ ($\mu$mole quanta $m^{-2}$ $s^{-1}$)$^{-1}$ | 0.093 ± 0.009 | 0.046 ± 0.004 | 0.014 ± 0.005 |
| $\overline{a}^*_\Phi$, $m^2$ mg Chl$a^{-1}$ | 0.021 ± 0.002 | 0.021 ± 0.001 | 0.038 ± 0.001 |
| $\phi_{Cmax}$, mole C mole quanta$^{-1}$ | 0.102 | 0.050 | 0.009 |

[a]Variable $\phi_{Cmax}$ is derived as the ratio of $\alpha^B$ by $\overline{a}^*_\Phi$, using appropriate conversions for the time units.

shows that only few environmental parameters correlate with $\Phi_{cmax}$, which makes this important variable difficult to predict. Other studies pointed out the difficulty to relate $\Phi_{cmax}$ variability to environmental forcing variables and consequently emphasized that quantum yield-based primary production models behave as poor predictors of primary production [*Siegel et al.*, 2001; *Sorensen and Siegel*, 2001]. In the present study, $\Phi_{cmax}$, which does not show any relationship with biotic and abiotic factors at any season (Table 3), is positively related to size (and to %micro) at the yearly scale (Figure 7, Table 4). The greater the size of the phytoplankton assemblage, the higher the value of $\Phi_{cmax}$. This result is not in agreement with observations, mostly conducted on laboratory controlled cultures of single species, where energetic efficiencies are considered to be independent of size [e.g., *Finkel*, 2001, and reference therein]. However, the present results demonstrate that, when large phytoplankton (diatoms) are present, $\Phi_{cmax}$ (and also $P^B_{max}$ and $\alpha^B$) is higher than for other phytoplankton communities. These results also suggest that size might be a good proxy for inferring changes in essential photophysiological properties like $\Phi_{cmax}$, $P^B_{max}$ and $\alpha^B$.

[37] In contrast to our observations made on $\Phi_{cmax}$ and $P^B_{max}$, the (negative) correlation between $\overline{a}^*_\Phi$ and size is an expected result (Table 4). The greater the size, the larger is the so-called packaging effect and the lower is the specific absorption coefficient [*Morel and Bricaud*, 1981]. The data presented here represent a subset of a larger data set which fully confirms, on natural samples and using the same pigment–size derived index, that $a^*$ is strongly dependent on cell size [*Bricaud et al.*, 2004].

### 4.3. Toward an Embedded Taxonomic-Dependent Parameterization of Bio-optical Models

[38] Several investigations have pointed out the possible role of changes in community composition as a possible driver of variations in photophysiological properties [*Cullen*, 1990; *Johnson and Howd*, 2000; *Sorensen and Siegel*, 2001]. Our observations show that community composition is also a good index of photophysiological properties. In fact, it integrates the combined effects of several abiotic factors, as well as possible species-specific properties.

[39] Therefore as an alternative to previous attempts to relate photophysiological properties of phytoplankton to abiotic factors, we proposed to develop a taxonomic-dependant parameterization of photosynthesis in bio-optical primary production models.

[40] In the same way as $\langle P \rangle$ was decomposed into partial production associated with each main phytoplankton size

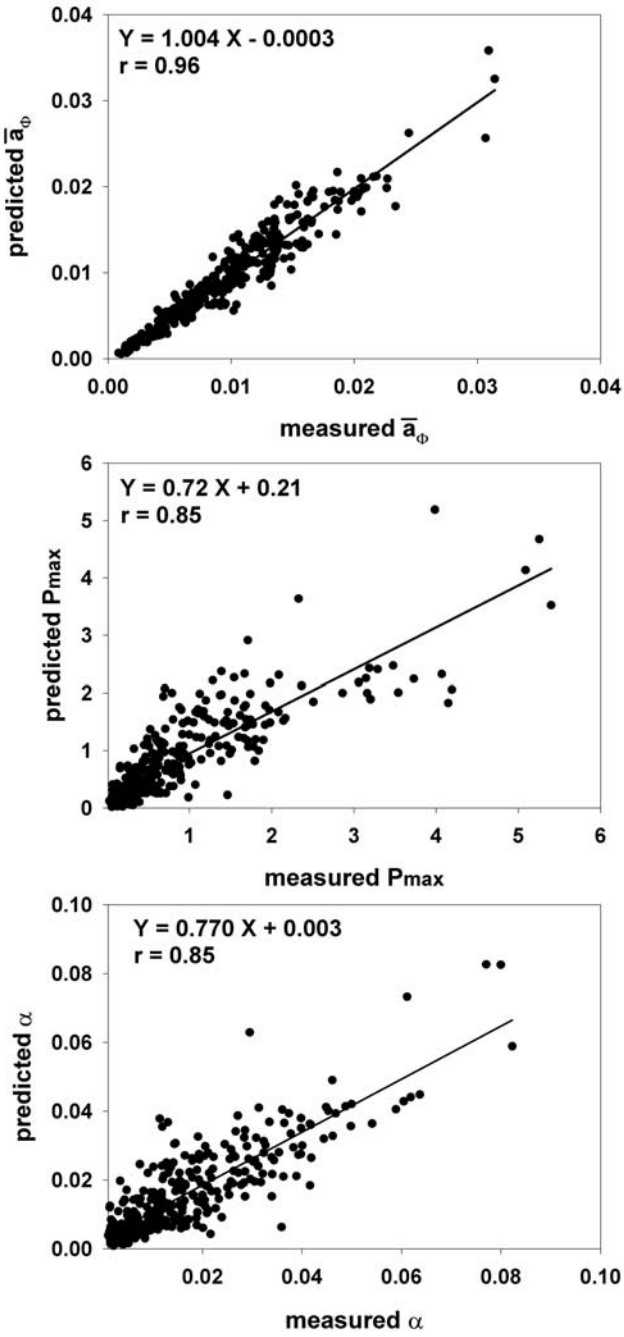


**Figure 8.** Comparison of measured and predicted values for three bio-optical or photophysiological parameters. Predicted values are calculated using coefficients derived from the multiple regression (Table 5).

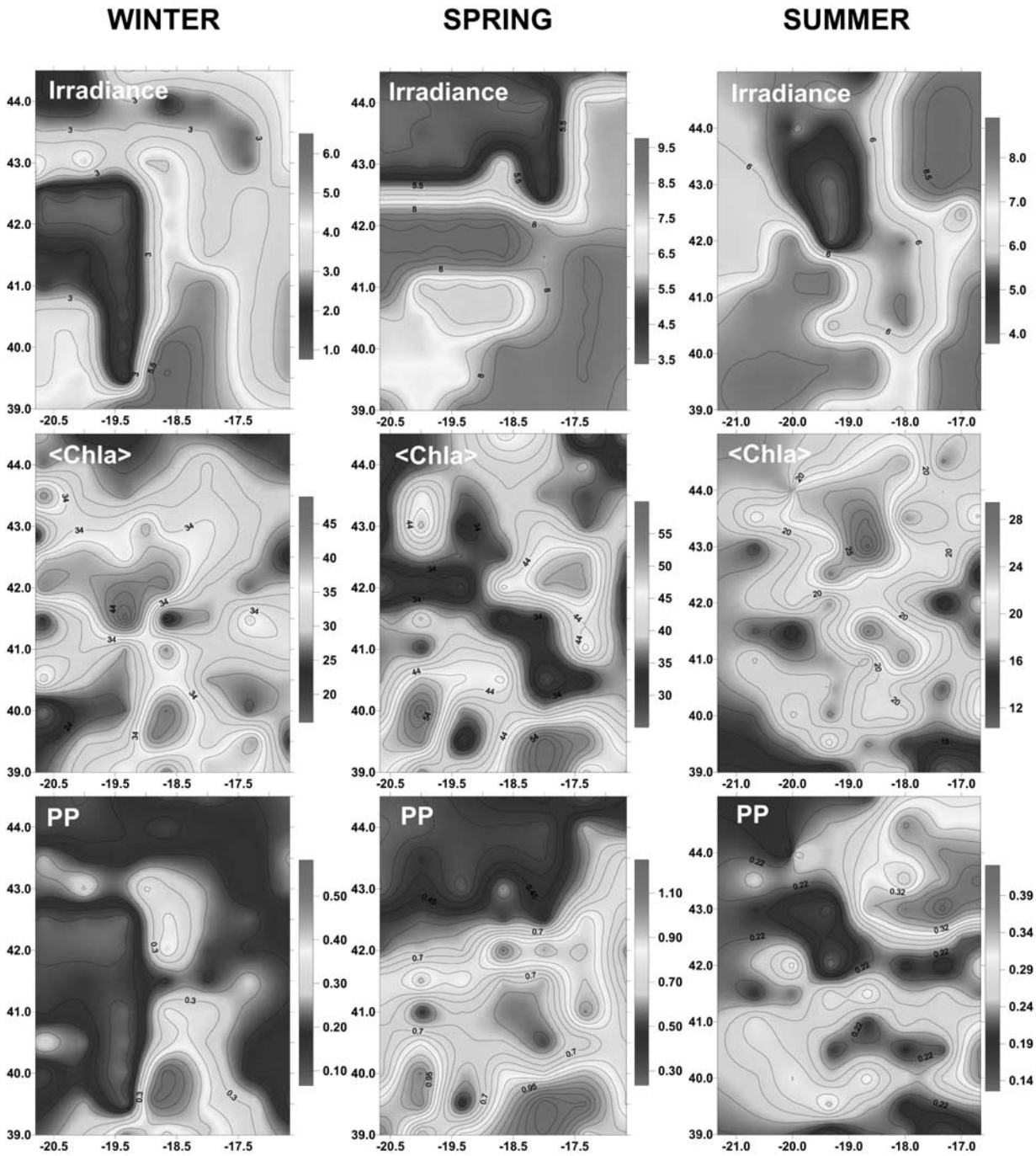


**Figure 9.** Spatial distribution of surface irradiance (MJ $m^{-2}$ $d^{-1}$) integrated chlorophyll *a* (mg Chla $m^{-2}$) content within the 1.5 *Ze* layer, $\langle \mathrm{Chl}a \rangle$, and primary production (gC $m^{-2}$ $d^{-1}$) at the three seasons investigated over the POMME area. See color version of this figure at back of this issue.

group (equation (6)), the main photophysiological or bio-optical properties can be decomposed as

$$X = [_{\mathrm{pico}}\mathrm{Chl}a]X^*_{\mathrm{pico}} + [_{\mathrm{nano}}\mathrm{Chl}a]X^*_{\mathrm{nano}} + [_{\mathrm{micro}}\mathrm{Chl}a]X^*_{\mathrm{micro}}, \quad (7)$$

where $X$ corresponds to a non-normalized quantity ($a$, $\alpha$ or $P_{\max}$) and $X^*$ represents the [Chl*a*]-normalized quantity associated with either pico-, nano-, or microphytoplankton. From equation (6), the estimation of $\Psi^*_{\mathrm{pico}}$, $\Psi^*_{\mathrm{nano}}$ $\Psi^*_{\mathrm{micro}}$ was possible through multiple regression because the integrated quantities $\langle {}_{\mathrm{pico}}\mathrm{Chl}a \rangle$, $\langle {}_{\mathrm{nano}}\mathrm{Chl}a \rangle$, and $\langle \mathrm{microChl}a \rangle$ were independent (LEG2). Here the volumetric concentration $[_{\mathrm{pico}}\mathrm{Chl}a]$, $[_{\mathrm{nano}}\mathrm{Chl}a]$, and $[_{\mathrm{micro}}\mathrm{Chl}a]$ acquired during LEG1 are not strictly independent as $[_{\mathrm{nano}}\mathrm{Chl}a]$, and

**Table 6.** Total and Size Class–Specific Primary Production Rates Derived Using the ψ*-Based Approach[a]

| | Winter | Spring | Summer |
|---|---|---|---|
| Primary production (clear sky irradiance) | 363 ± 94 | 939 ± 223 | 393 ± 80 |
| Primary production (measured irradiance) | 218 ± 109 | 660 ± 240 | 259 ± 66 |
| Micro PP | 31 ± 18 | 201 ± 132 | 35 ± 36 |
| Nano PP | 103 ± 54 | 370 ± 152 | 111 ± 36 |
| Pico PP | 85 ± 40 | 90 ± 54 | 113 ± 31 |

[a]See text. Production rates are in mgC $m^{-2}$ $d^{-1}$.

[$_{micro}$Chl*a*] showed some degree of correlation. Thus the partial coefficients derived by multiple regression are only indicative (Table 5). The trends reported in section IV.2 are nevertheless confirmed. As expected, the specific absorption coefficient of picophytoplankton appears to be the highest. Similarly and as expected from Figure 7 ($P^B_{max}$ versus size), $P^B_{max}$ would be higher for microphytoplankton than for picophytoplankton. The same observation is made for $\alpha^B$ and for the derived quantity $\Phi_{Cmax}$ (ratio of specific $\alpha^B$ by specific $\overline{a}^*_\Phi$). Using the estimation of the size group–specific $\overline{a}^*_\Phi$, $P^B_{max}$ and $\alpha^B$ coefficients, the prediction of $\overline{a}^*_\Phi$, $P_{max}$ and $\alpha$ on the basis from the volumetric concentration [$_{pico}$Chl*a*], [$_{nano}$Chl*a*], and [$_{micro}$Chl*a*] is highly satisfactory (Figure 8).

[41] The present observations are in close agreement with the Ψ* based approach: the larger the phytoplankton, the lower its efficiency in light capture (result already known) and the higher its efficiency for carbon fixation (at both low and high irradiances). It should be noted that, when environmental conditions appear most favorable, likely in spring, diatoms (and also nanoplankton) are at maximum of their abundance and more generally, the size of the phytoplankton assemblage is at its highest.

### 4.4. Seasonal Biomass and Production Budget of the POMME Area

[42] The large pigment data set acquired during the first LEGs of the three cruises (~80 HPLC stations each time) allows a description of phytoplankton pigment distribution with an unprecedented spatial resolution for such a large area. When size class–specific [Chl*a*] derived from this data set are combined to measured surface irradiance, primary production rates (total and specific) can be estimated through the use of equation (6) for all stations of the sampling grid (Figure 9) and seasonal trends can be inferred (Table 6).

[43] Overall, irradiance has a highly significant impact on primary production estimates that do not necessarily mirror the biomass fields (Figure 9). For example, as a consequence of extremely low surface irradiance (~1 MJ $m^{-2}$ $d^{-1}$) in winter in the western part of the area, low primary production rates were estimated (<100 mg C $m^{-2}$ $d^{-1}$) despite high phytoplankton biomass (>40 mg Chl*a* $m^{-3}$) (Figure 9). In general, the range of variation in daily irradiance (factor of 6.3, 2.8, 2.3 between extreme values in winter, spring and summer, respectively, see also Figure 1) is higher or comparable to that of ⟨Chl*a*⟩ (3.2, 2.4, 2.9) which makes primary production rates equally dependant on both variables. On average, the reduction of primary production due to cloudiness as compared to maximal (potential) production by clear sky is 40% in winter, 30% in spring and 25% in summer (Table 6). However, local depression of primary production rates of up to 84% can be recorded for extremely cloudy winter days.

[44] During summer, the highest primary production rates are recorded in the north eastern part of the POMME area; actually these high rates are not associated to high biomass. If size class–specific rates of primary production are analyzed (Figure 10), the southern part of this high primary production zone is clearly associated with a tongue of enhanced microphytoplankton production, which has a higher Ψ* than other groups (Table 2). Close examination of the pigment data show that, for this particular zone, dinoflagellates (peridinin) and not diatoms (fucoxanthin) dominate this microphytoplankton assemblage. This microphytoplankton "spot" is located in a cyclonic structure, $C_{31}$, highlighted from numerical simulation coupled to assimilation of altimetry and CTD data [*Mémery et al.*, 2005, Figure 2]. Such cyclonic structures are expected to support nutrient fueling into the euphotic layer in such stratified systems [*McGillicuddy et al.*, 1999].

[45] In winter and as a consequence of a rather constant composition of the phytoplankton community over the whole POMME area, group-specific rates of primary production mirror the total rates. The highest values are recorded in close association with the anticyclonic structure $A_2$ [*Mémery et al.*, 2005, Figure 2]. At the time of the spring bloom, this structure has drifted to the South Western part of the POMME area. It is now clearly associated with a dominance of diatoms which drive up to 65% of the carbon fixation. East of this anticyclonic structure and associated with the jet/front system surrounding it, primary production rates are mainly due to nanophytoplankton (62%). These observations demonstrate that during the initiation and the development of the spring bloom, the qualitative nature of the phytoplankton assemblage and of resulting carbon fixation appear spatially variable. Whether this apparent variability results from mesoscale dynamics or from a temporal evolution remains nevertheless to be documented.

## 5. Conclusion and Perspectives

[46] An essential outcome of the present study is that a potential alternative does exist for bio-optical models which try to mechanistically relate photophysiological parameters to environmental forcing variables [*Behrenfeld et al.*, 2002]. We suggest that these parameters can also be indexed on the composition of the phytoplankton community. This composition can indeed be considered as the ultimate integrator of the environmental forcing variables (and of their complex interactions) occurring over a variety of spatial and temporal scales.

[47] To our best knowledge, the present study is one of the few that addresses bio-optical model parameterization using such an approach. To be further evaluated, it definitely requires that in situ studies be designed to establish local, regional and global databases of simultaneously determined taxonomic composition (e.g., HPLC), photophysiological parameters (*P* versus *E* curves) and phytoplankton absorption. To date, such databases are too scarce. This data paucity is the one important reason why the photophysiological status of phytoplankton communities has essentially been

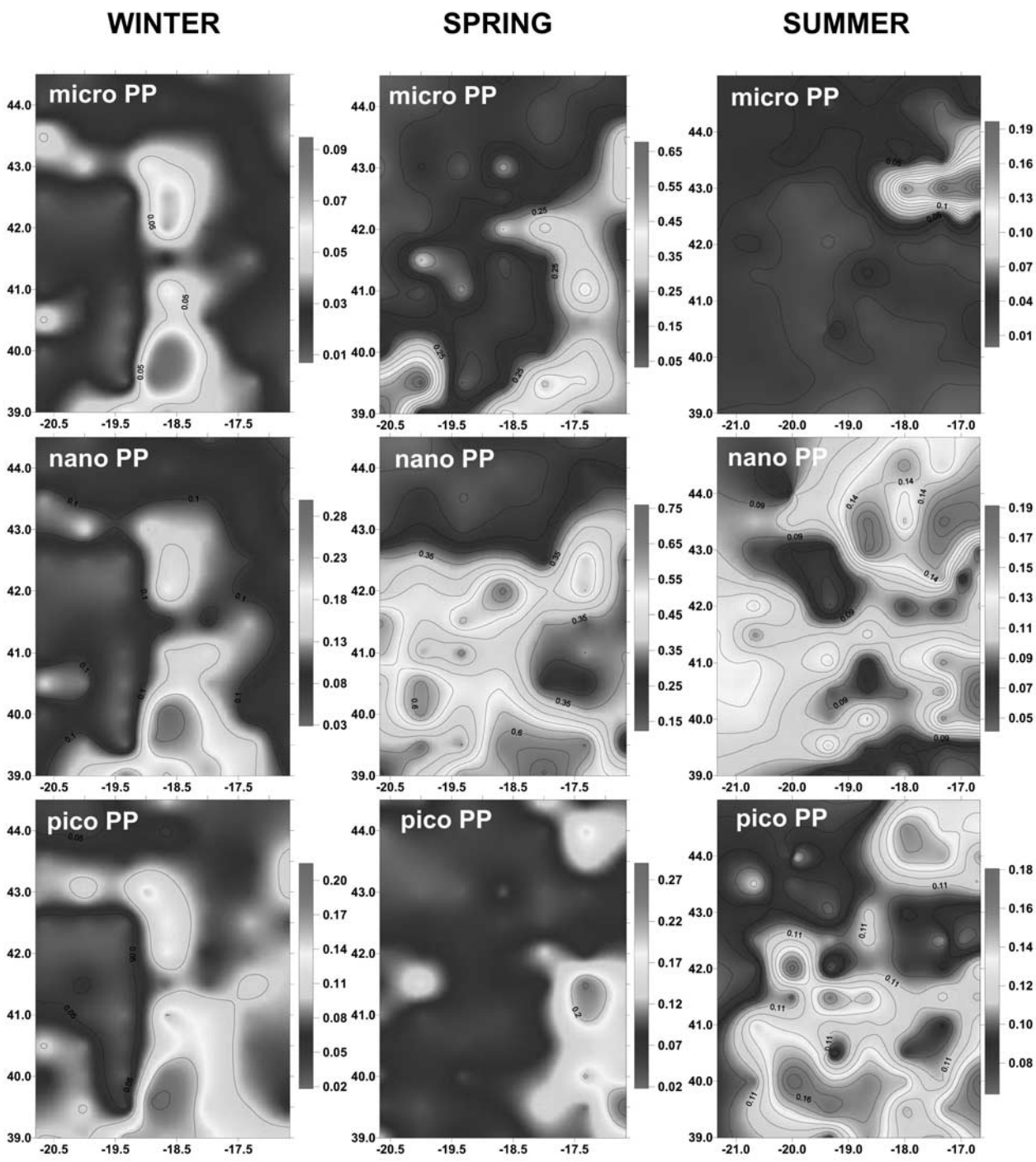


**Figure 10.** Spatial distribution of primary production (gC $m^{-2}$ $d^{-1}$) associated with each phytoplankton size class at the three seasons investigated over the POMME area. See color version of this figure at back of this issue.

analyzed with respect to standard core environmental variables (light, nutrients, temperature).

[48] Evidence is arising that the size structure or composition of phytoplankton communities is amenable to a certain degree of estimation at the global scale, from remotely sensed [Chl*a*] (Uitz et al., submitted manuscript, 2005). If the trends highlighted in the present study become confirmed with the availability of more data, the use of bio-optical models with embedded taxonomic composition parameterization may thus be generalized at the global scale. Such models would present a significant improvement over more traditional bio-optical models. Not only would primary production rates be more accurately determined, but specific rates of primary production for phytoplankton classes or functional groups could be ultimately derived. Such quantities are essential to feed a new class of

biogeochemical, climatically relevant models, which explicitly consider several phytoplankton functional types [*Lequéré et al.*, 2005].

[49] **Acknowledgments.** The PIs of the POMME program, Laurent Mémery and Gilles Reverdin, are warmly acknowledged for their deep investment in all phases of the project and especially to have allowed us to have access to a unique sampling platform in 2001. Nutrient data were kindly provided by Camilla Fernandez and Patrick Raimbault. The present contribution was essentially supported by the PROOF program (http://www.obs-vlfr.fr/proof).

## References

Antoine, D., and A. Morel (1996), Oceanic primary production: 1. Adaptation of a spectral light-photosynthesis model in view of application to satellite chlorophyll observations, *Global Biogeochem. Cycles*, *10*, 43–56.

Babin, M. (1994), An incubator designed for extensive and sensitive measurements of phytoplankton photosynthetic parameters, *Limnol. Oceanogr.*, *39*, 694–702.

Babin, M., A. Morel, H. Claustre, A. Bricaud, Z. Kolber, and P. G. Falkowski (1996), Nitrogen- and irradiance-dependent variations of the maximum quantum yield of carbon fixation in eutrophic, mesotrophic and oligotrophic marine systems, *Deep Sea Res., Part I*, *43*, 1241–1272.

Behrenfeld, M. J., and P. G. Falkowski (1997), Photosynthetic rates derived from satellite-based chlorophyll concentration, *Limnol. Oceanogr.*, *42*, 1–20.

Behrenfeld, M. J., E. Manaron, D. A. Siegel, and S. B. Hooker (2002), Photoacclimation and nutrient-based model of light-saturated photosynthesis for quantifying oceanic primary production, *Mar. Ecol. Prog. Ser.*, *228*, 103–117.

Bouman, H. A., T. Platt, S. Sathyendranath, W. K. W. Li, V. Stuart, C. Fuentes-Yaco, H. Maass, E. P. W. Horne, O. Ulloa, V. A. Lutz, and M. Kyewalyanga (2003), Temperature as indicator of optical properties and community structure of marine phytoplankton: Implications for remote sensing, *Mar. Ecol. Prog. Ser.*, *258*, 19–30.

Bricaud, A., M. Babin, A. Morel, and H. Claustre (1995), Variability in the chlorophyll-specific absorption coefficients of natural phytoplankton: Analysis and parameterization, *J. Geophys. Res.*, *100*, 13,321–13,332.

Bricaud, A., H. Claustre, J. Ras, and K. Oubelkheir (2004), Natural variability of phytoplanktonic absorption in oceanic waters: Influence of the size structure of algal populations, *J. Geophys. Res.*, *109*, C11010, doi:10.1029/2004JC002419.

Bustillos-Guzman, J., H. Claustre, and J. C. Marty (1995), Specific phytoplankton signatures and their relationship to hydrographic conditions in the coastal northwestern Mediterranean Sea, *Mar. Ecol. Prog. Ser.*, *124*, 247–258.

Caniaux, G., A. Brut, D. Bourras, H. Giordani, A. Paci, L. Prieur, and G. Reverdin (2005), A 1 year sea surface heat budget in the northeastern Atlantic basin during the POMME experiment: 1. Flux estimates, *J. Geophys. Res.*, *110*, C07S02, doi:10.1029/2004JC002596.

Chisholm, S. W. (1992), Phytoplankton size, in *Primary Productivity and Biogeochemical Cycles in the Sea*, edited by P. G. Falkowski and A. D. Woodhead, pp. 213–247, Springer, New York.

Claustre, H. (1994), The trophic status of various oceanic provinces as revealed by phytoplankton pigment signatures, *Limnol. Oceanogr.*, *39*, 1206–1210.

Claustre, H., M. A. Moline, and B. B. Prézelin (1997), Sources of variability in the column photosynthetic cross section of Antarctic coastal waters, *J. Geophys. Res.*, *102*, 25,047–25,060.

Claustre, H., F. Fell, K. Oubelkheir, L. Prieur, A. Sciandra, B. Gentili, and M. Babin (2000), Continuous monitoring of surface optical properties across a geostrophic front: Biogeochemical inferences, *Limnol. Oceanogr.*, *45*, 309–321.

Claustre, H., et al. (2004), An intercomparison of HPLC phytoplankton pigment methods using in situ samples: Application to remote sensing and database activities, *Mar. Chem.*, *85*, 41–61.

Cleveland, J. S., M. J. Perry, D. A. Kiefer, and M. C. Talbot (1989), Maximum quantum yield of photosynthesis in the northwestern Sargasso Sea, *J. Mar. Res.*, *47*, 869–886.

Cullen, J. J. (1990), On models of growth and photosynthesis in phytoplankton, *Deep Sea Res., Part A*, *37*, 667–683.

Falkowski, P. G. (1981), Light-shade adaptation and assimilation numbers, *J. Plankton Res.*, *3*, 203–216.

Fernández, C. I., P. Raimbault, N. Garcia, P. Rimmelin, and G. Caniaux (2005), An estimation of annual new production and carbon fluxes in the northeast Atlantic Ocean during 2001, *J. Geophys. Res.*, *110*, C07S13, doi:10.1029/2004JC002616.

Finkel, Z. V. (2001), Light absorption and size scaling of light-limited metabolism in marine diatoms, *Limnol. Oceanogr.*, *46*, 86–94.

Geider, R. J., H. L. MacIntyre, and T. M. Kana (1996), A dynamic model of photoadaptation in phytoplankton, *Limnol. Oceanogr.*, *41*, 1–15.

Gieskes, W. W. C., G. W. Kraay, A. Nontji, D. Setiapermana, and Sutomo (1988), Monsoonal alternation of a mixed and a layered structure in the phytoplankton of the euphotic zone of the Banda Sea (Indonesia): A mathematical analysis of algal pigment fingerprints, *Neth. J. Sea Res.*, *22*, 123–137.

Hashimoto, S., and A. Shiomoto (2002), Light utilization efficiency of size-fractionated phytoplankton in the subarctic Pacific, spring and summer 1999: High efficiency of large-sized diatom, *J. Plankton Res.*, *24*, 83–87.

Johnson, Z., and P. Howd (2000), Marine photosynthetic performance forcing and periodicity for the Bermuda Atlantic Time Series, 1989–1995, *Deep Sea Res., Part I*, *47*, 1485–1512.

Lequéré, C., et al. (2005), Strengths and limitation of Dynamic Green Ocean models based on phytoplankton functional types, *Global Change Biol.*, in press.

Mackey, M. D., D. J. Mackey, H. W. Higgins, and S. W. Wright (1996), CHEMTAX—A program for estimating class abundances from chemical markers: Application to HPLC measurements of phytoplankton, *Mar. Ecol. Prog. Ser.*, *144*, 265–283.

Maranon, E., M. J. Behrenfeld, N. Gonzalez, B. Mourino, and M. V. Zubkov (2003), High variability of primary production in oligotrophic waters of the Atlantic Ocean: Uncoupling from phytoplankton biomass and size structure, *Mar. Ecol. Prog. Ser.*, *257*, 1–11.

McGillicuddy, D. J., Jr., R. Johnson, D. A. Siegel, A. F. Michaels, N. R. Bates, and A. H. Knap (1999), Mesoscale variations of biogeochemical properties in the Sargasso Sea, *J. Geophys. Res.*, *104*, 13,381–13,394.

Mémery, L., G. Reverdin, J. Paillet, and A. Oschlies (2005), Introduction to the POMME special section: Thermocline ventilation and biogeochemical tracer distribution in the northeast Atlantic Ocean and impact of mesoscale dynamics, *J. Geophys. Res.*, doi:10.1029/2005JC002976, in press.

Morel, A. (1991), Light and marine photosynthesis: A spectral model with geochemical and climatological implications, *Prog. Oceanogr.*, *26*, 263–306.

Morel, A., and J. F. Berthon (1989), Surface pigments, algal biomass profiles, and potential production of the euphotic layer: Relationships reinvestigated in view of remote-sensing applications, *Limnol. Oceanogr.*, *34*, 1545–1562.

Morel, A., and A. Bricaud (1981), Theoretical results concerning light absorption in a discrete medium, and application to specific absorption of phytoplankton, *Deep Sea Res., Part A*, *28*, 1375–1393.

Morel, A., and S. Maritorena (2001), Bio-optical properties of oceanic waters: A reappraisal, *J. Geophys. Res.*, *106*, 7163–7180.

Morel, A., and R. C. Smith (1974), Relation between total quanta and total energy for aquatic photosynthesis, *Limnol. Oceanogr.*, *19*, 591–600.

Morel, A., D. Antoine, M. Babin, and Y. Dandonneau (1996), Measured and modeled primary production in the northeast Atlantic (EUMELI JGOFS program): The impact of natural variations in photosynthetic parameters on model predictive skill, *Deep Sea Res., Part I*, *43*, 1273–1304.

Moutin, T., and P. Raimbault (2002), Primary production, carbon export and nutrients availability in western and eastern Mediterranean Sea in early summer 1996, *J. Mar. Syst.*, *33–34*, 273–298.

Paillet, J., and M. Arhan (1996), Shallow pycnoclines and mode waters subduction in the eastern North Atlantic, *J. Phys. Oceanogr.*, *26*, 96–114.

Parsons, T. R., Y. Maita, and C. M. Lalli (1984), Photosynthesis as measured by the uptake of radioactive carbon, in *A Manual of Chemical and Biological Methods for Seawater Analyses*, edited by R. Maxwell, pp. 115–120, Elsevier, New York.

Partensky, F., W. R. Hess, and D. Vaulot (1999), *Prochlorococcus*, a marine photosynthetic prokaryote of global significance, *Microbiol. Mol. Biol. Rev.*, *63*, 106–127.

Platt, T., and S. Sathyendranath (1988), Oceanic primary production: Estimation by remote sensing at local and regional scales, *Science*, *241*, 1613–1620.

Platt, T., C. L. Gallegos, and W. G. Harrison (1980), Photoinhibition of photosynthesis in natural assemblages of marine phytoplankton, *J. Mar. Res.*, *38*, 687–701.

Sakshaug, E., K. Andresen, and D. A. Kiefer (1989), A steady state description of growth and light absorption in the marine planktonic diatom *Skeletonema costatum*, *Limnol. Oceanogr.*, *34*, 198–205.

Siegel, D. A., T. K. Westberry, M. C. O'Brien, N. B. Nelson, A. F. Michaels, J. R. Morrison, A. Scott, E. A. Caporelli, J. C. Sorensen,

and S. Maritorena (2001), Bio-optical modeling of primary production on regional scales: The Bermuda BioOptics project, *Deep Sea Res., Part II*, *48*, 1865–1896.

Siegel, D. A., S. C. Doney, and J. A. Yoder (2002), The North Atlantic spring phytoplankton bloom and Sverdrup's critical depth hypothesis, *Science*, *296*, 730–733.

Sorensen, J. C., and D. A. Siegel (2001), Variability of the effective quantum yield for carbon assimilation in the Sargasso Sea, *Deep Sea Res., Part II*, *48*, 2005–2035.

Stramski, D., A. Sciandra, and H. Claustre (2002), Effect of temperature, nitrogen, and light limitation on the optical properties of the marine diatom *Thalassiosira pseudonana*, *Limnol. Oceanogr.*, *47*, 392–403.

Vidussi, F., H. Claustre, J. Bustillos-Guzman, C. Cailliau, and J. C. Marty (1996), Determination of chlorophylls and carotenoids of marine phytoplankton: Separation of chlorophyll *a* from divinyl-chlorophyll *a* and zeaxanthin from lutein, *J. Plankton Res.*, *18*, 2377–2382.

Vidussi, F., H. Claustre, B. B. Manca, A. Luchetta, and J.-C. Marty (2001), Phytoplankton pigment distribution in relation to upper thermocline circulation in the eastern Mediterranean Sea during winter, *J. Geophys. Res.*, *106*, 19,939–19,956.

Wozniak, B., J. Dera, and O. Koblentz-Mishke (1992), Modeling the relationship between primary production, optical properties and nutrients in the sea (as a basis for indirectely estimating primary production), *Proc. SPIE Soc. Opt. Eng.*, *11*, 246–275.

---

M. Babin, H. Claustre, S. Dallot, D. Merien, L. Prieur, and J. Ras, Observatoire Océanologique de Villefranche, Laboratoire d'Océanographie de Villefranche, UMR 7093, B.P. 08, F-06238 Villefranche-sur-mer, France. (marcel@obs-vlfr.fr; claustre@obs-vlfr.fr; dallot@obs-vlfr.fr; merien@obs-vlfr.fr; prieur@obs-vlfr.fr; jras@obs-vlfr.fr)

H. Dousova and O. Prasil, Photosynthesis Research Center, Institute of Microbiology AVCR and University of South Bohemia, Opatovicky mlyn, 37981 Trebon, Czech Republic. (dousova@alga.cz; prasil@alga.cz)

T. Moutin, Laboratoire d'Océanographie et de Biogéochimie, UMR 6535, Centre d'Océanologie de Marseille, Campus de Luminy, Case 901, F-13288 Marseille cedex 09, France. (thierry.moutin@com.univ-mrs.fr)

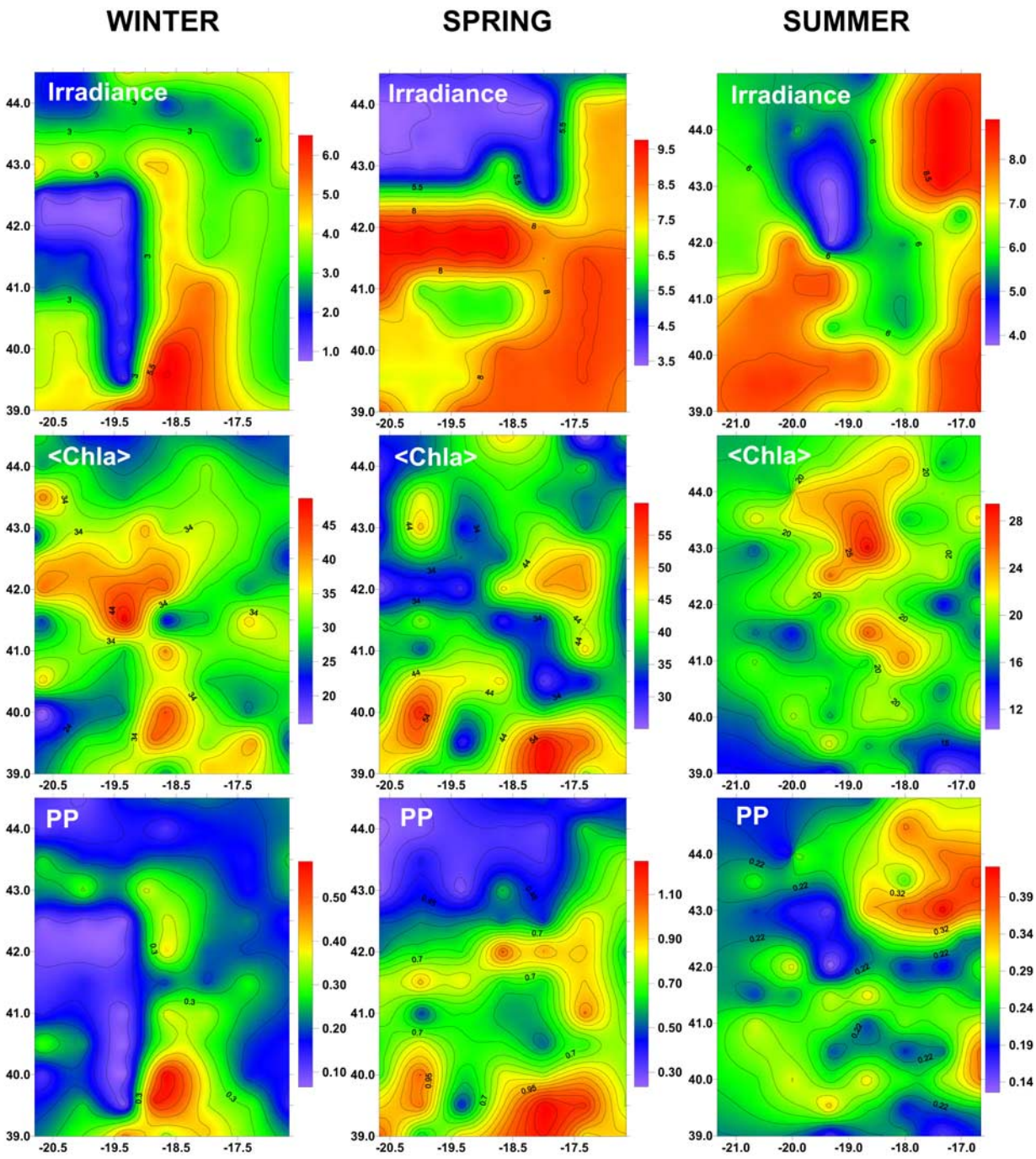


**Figure 9.** Spatial distribution of surface irradiance (MJ $m^{-2}$ $d^{-1}$) integrated chlorophyll *a* (mg Chla $m^{-2}$) content within 1.5*Ze* layer, $\langle$Chl*a*$\rangle$, and primary production (gC $m^{-2}$ $d^{-1}$) at the three seasons investigated over the POMME area.

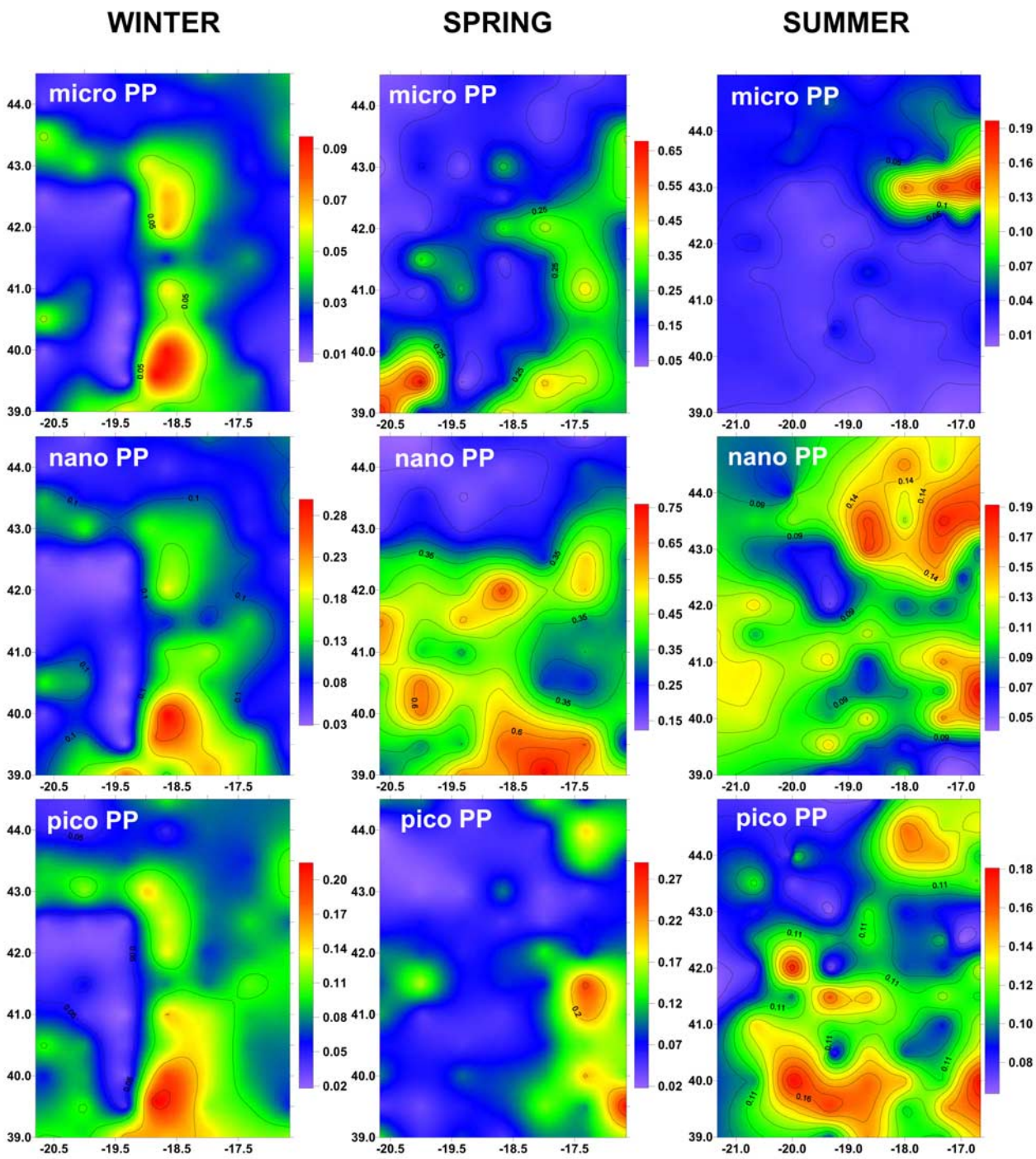


**Figure 10.** Spatial distribution of primary production (gC $m^{-2}$ $d^{-1}$) associated with each phytoplankton size class at the three seasons investigated over the POMME area.